

Rethinking Divisive Hierarchical Clustering from a Distributional Perspective

Kaifeng Zhang, Kai Ming Ting, Tianrun Liang, Qiuran Zhao

January 28, 2026

Abstract

We uncover that current objective-based Divisive Hierarchical Clustering (DHC) methods produce a dendrogram that does not have three desired properties i.e., no unwarranted splitting, group similar clusters into a same subset, ground-truth correspondence. This shortcoming has their root cause in using a set-oriented bisecting assessment criterion. We show that this shortcoming can be addressed by using a distributional kernel, instead of the set-oriented criterion; and the resultant clusters achieve a new distribution-oriented objective to maximize the total similarity of all clusters (TSC). Our theoretical analysis shows that the resultant dendrogram guarantees a lower bound of TSC. The empirical evaluation shows the effectiveness of our proposed method on artificial and Spatial Transcriptomics (bioinformatics) datasets. Our proposed method successfully creates a dendrogram that is consistent with the biological regions in a Spatial Transcriptomics dataset, whereas other contenders fail.

1 Introduction

Hierarchical clustering (HC) seeks to explore the relationships between clusters at various levels of granularity. HC is extensively applied [LBWX19, TLM10, PZZ⁺22, SJJ⁺22, DBE⁺15, FZCW21] due to its hierarchical structure named dendrogram, which uncovers the pattern of clusters and their subclusters in a given dataset.

HC is categorized into two types: Agglomerative Hierarchical Clustering (AHC) and Divisive Hierarchical Clustering (DHC) [CAKMTM19]. AHC works in a bottom-up manner. It initially groups the closest pair of points according to a linkage function and progressively merges the two nearest subclusters until all the points are in one cluster. DHC works in a top-down manner. It starts with all points in one cluster and successively partitions them into smaller clusters according to some bisecting assessment criterion.

The core problem in objective-based DHC in building a dendrogram T is how to bisect a set of data points into two subsets at each internal node of T . By *treating each cluster as a set of points*, it requires a set-oriented bisecting assessment criterion to perform each bisecting. We show here that an optimized dendrogram, though meeting the stated objective of a DHC method, can be a poor dendrogram that does not possess certain desirable properties. We show that this is because the entire process ignores the distributional information in a dataset.

As the root cause is due to the use of a *set-oriented* bisecting assessment criterion, we propose an alternative *distribution-oriented* approach where each cluster is treated as independent and identically distributed (i.i.d.) points generated from a distribution (which characterizes the shape, size, and density of the ground-truth cluster). The resultant objective-based DHC method is derived from a distributional kernel, and it succeeds in producing a dendrogram with three desired properties (see the next paragraph), and the clusters produced satisfy a new distribution-oriented objective. In addition, we show that this new approach has $O(n)$ time complexity.

The proposed new objective-based DHC has the following unique features: (i) It is the first objective-based DHC, named H- $\mathcal{K}C$, which has the objective function defined based on a distributional kernel \mathcal{K} . (ii) The bisecting employs the same distributional kernel as used in the objective function. This is unlike the current objective-based DHC in two aspects. First, our proposed method does not need a set-oriented bisecting assessment criterion. Second, the set-oriented bisecting assessment criterion used in existing DHC methods has no direct relationship to its objective function. (iii) H- $\mathcal{K}C$ runs in linear

time. In contrast, the current fastest objective-based DHC has nearly linear time only if a similarity graph is given (which often requires quadratic time to construct). (iv) It is a distribution-oriented algorithm that discovers clusters of arbitrary shapes, sizes and densities. (v) The dendrogram produced by H-*KC* possesses **three desired properties: no unwarranted cluster splitting, group similar clusters into a same subset, ground-truth correspondence** (see Section 3 for details), whereas other existing methods fail to do so.

Our contributions are:

1. Identifying the root cause of the shortcoming of existing objective-based DHC: the use of a set-oriented bisecting assessment criterion.
2. Creating a new distribution-oriented approach to the objective-based DHC problem.
3. Proposing a new objective-based DHC algorithm using the distribution-oriented approach called H-*KC* that produces a dendrogram with three desired properties.
4. Establishing the theoretical guarantee that H-*KC* is an objective-based DHC, and it produces a dendrogram which has lower bounded a global objective (i.e., the dendrogram is guaranteed to have a certain quality).
5. Conducting empirical evaluations comparing different objective-based DHC algorithms on artificial and Spatial Transcriptomics (bioinformatics) datasets.

2 Related Work

Early DHC methods produce a dendrogram that does not base on an objective function. Examples of non-objective-based methods are as follows. Two earliest methods perform bisecting based on seed selection [MSWDM64, Hub73]. PDDP [Bol98] uses a linear boundary to split the data in one principal direction. DIANA [KR90] performs bisecting by mimicking the way a political party might split up due to inner conflicts. It separates a point which is least similar to its own cluster as the initial seed of a new cluster, and then it moves points from the old cluster to the new cluster if they are more similar to this new one.

An early DHC called Bisect-Kmeans [SKK00] performs optimization on each split. It is later identified to be an objective-based DHC by using Kmeans to select the best split with the least total sum of squared errors. WM20 proves that Bisect-Kmeans approximates the Revenue Objective of a given dataset X , which is defined to be $rev(X) = \sum_{S \rightarrow (S_1, S_2) \in T} \sum_{x \in S_1, y \in S_2} rev(x, y)$, where $S \rightarrow (S_1, S_2) \in T$ means all the splits in dendrogram T , $rev(x, y) = \min\{\frac{d(x, y)}{\max\{d(x, \rho(S_1)), d(y, \rho(S_2))\}}, 1\}$, $\rho(S)$ is the center of S , and d is Euclidean distance.

Other works on objective-based hierarchical clustering [Das16, RP17, CNC18, GPvL19] focus on producing a dendrogram T that has the smallest Dasgupta cost function. Given an undirected graph $\mathbf{G} = (V, E, w)$ with $|V|$ vertices, $|E|$ edges connecting two vertices $u, v \in V$, and similarity function $w : V \times V \rightarrow \mathbb{R}_{\geq 0}$, the Dasgupta cost function of T produced from \mathbf{G} is given as follows [Das16]: $cost_{\mathbf{G}}(T) = \sum_{\{u, v\} \in E} w(u, v) \times |LCA_T(u, v)|$, where $LCA_T(u, v)$ denotes the lowest common ancestor of u and v in T . A variant of Dasgupta cost function is CKMM objective [CAKMT17, NYA21], which basically replaces similarity $w(u, v)$ with distance $d(u, v)$; and minimizing Dasgupta cost is replaced with maximizing CKMM.

A recent work SpecWRSC [LMS23] uses Spectral Clustering to produce a set of clusters and then builds a dendrogram from these clusters. It produces an $\mathcal{O}(1)$ -approximate tree of Dasgupta cost function in nearly-linear time relative to the size of the input graph (excluding the cost of building the adjacency matrix of the graph). This is achieved by using the set-oriented bisecting assessment criterion (sparsest-cut) which focuses solely on minimizing the sparsity between two subsets, i.e., $Sparsity(Y) = \frac{W(Y, V \setminus Y)}{|Y| \cdot |V \setminus Y|}$, where $W(Y, Z) = \sum_{u \in Y, v \in Z} w(u, v)$. While effective for the global objective, it tends to separate a cluster from the rest at each split (Figure 1c), failing to group similar clusters.

Current methods assess the quality of a split based on either the cohesiveness of each individual subset (e.g., Bisect-Kmeans) or the dissimilarity between the two resulting subsets (e.g., SpecWRSC), i.e. set-oriented bisecting assessment criterion. They can not consider the distributional information inside the subsets.

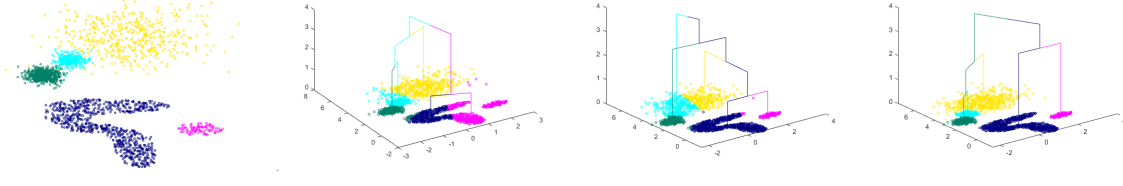


Figure 1: Dendrograms of Bisect-Kmeans, SpecWRSC and H- \mathcal{KC} on the artificial dataset which contains clusters of arbitrary shapes and varied densities. ϕ is Dendrogram Purity [HG05] (see the details in Appendix A.3).

In contrast, our proposed method uses a distributional kernel to build a dendrogram such that similar clusters are in either subset of each split (i.e., no similar clusters are split into different subsets). Its objective function is the total similarity of all clusters (TSC) in terms of the distributional kernel, which is used for the first time in hierarchical clustering. This function is similar to that used in an existing flat clustering method called Point-Set Kernel Clustering (psKC) [TWZ23], but psKC’s objective function is TSC in terms of point-set kernel. The difference between the two kernels and the details of psKC are provided in Appendix D.1.

Current evaluation methods on dendrograms have largely focused on minimizing cost and employed the commonly used Dendrogram Purity (DP) [HG05, KMKM17]. Yet, it has been revealed that ‘perfect DP can be achieved when each ground-truth cluster corresponds to a subtree, regardless of hierarchy on top or inside of the subtrees’ [NYA21]. In other words, DP does not reflect the quality of a dendrogram. Hence, in addition to DP, we compare the structures of dendrograms produced by different algorithms through visualization.

3 Desired Properties of a Dendrogram

Compared to flat clustering, a dendrogram provides the nested relationship between a cluster and its subclusters. The desired properties of a good dendrogram are:

1. **No unwarranted splitting:** A cluster should not be split into two sub-clusters in child nodes of a dendrogram if the cluster is not already at one node by itself.
2. **Group similar clusters into a same subset:** Every split in a dendrogram shall produce two subsets such that each subset contains clusters which are closer to each other than clusters in the other subset.
3. **Ground-truth correspondence:** Each leaf node of a dendrogram corresponds to a single cluster in a given dataset. This hierarchical clustering outcome is equivalent to the best outcome of a flat clustering.

3.1 Current Methods Fail to Yield a Dendrogram with All Desired Properties Mainly Due to The Set-Oriented Bisecting Assessment Criterion Employed

It is interesting to note that existing objective-based DHC methods produce a dendrogram which does not possess all the three properties, described in the following paragraphs.

The first desired property depends heavily on the ability to detect clusters of complex shapes, different data sizes and varied densities. And the third property is a natural consequence of the first one. Kmeans is known for its inability to find clusters of arbitrary shapes. For example, in a dataset with a L-shaped cluster, shown in Figure 1b, Bisect-Kmeans splits this cluster into two sub-clusters before it is in one node by itself, where the top left part of the L-shaped cluster is split in the first bisecting.

SpecWRSC relies on Spectral Clustering [VL07] for initialization, which lacks the first property due to its known difficulty in detecting clusters of varied densities [NG06]. As a result, it fails to identify

the three Gaussian distributions, incorrectly splitting the sparse right cluster and merging it with the dense middle one (Figure 1c).

The second desired property demands that the bisecting considers the similarity of clusters within each subset of the split. Conceptually, Bisect-Kmeans utilizes a bisecting assessment criterion that does not take into account the similarity of clusters within each subset of the split because it is set-oriented. Bisect-Kmeans chooses a split which minimizes the total sum of squared distance from the two mean vectors of the two subsets. Though it considers the cohesiveness in each subset, it is examined with respect to the mean vector only. Each of the mean vectors is often a poor representative of different clusters in either subsets of the split.

A key limitation of SpecWRSC is that it yields undesirable dendograms even with optimal initial clustering (e.g., psKC as shown in Appendix D.2). This is inherent to its bisecting assessment criterion, which tends to separate one cluster from the rest at each step, resulting in an unbalanced tree that fails to group similar clusters. This is also reflected in Figure 1c where SpecWRSC produces a highly unbalanced tree which separates one cluster from the rest at each internal node. In addition, the yellow cluster is less similar to the green and L-shaped clusters than the light blue cluster. Yet, the first split of SpecWRSC separates the light blue cluster and groups the yellow, green and L-shaped clusters together in one subset.

Both Bisect-Kmeans and SpecWRSC rely on set-oriented bisecting assessment criterion to determine the best split that does not ascertain that (a) similar clusters are grouped into a same subset, and (b) no individual clusters are split in any bisecting before each cluster is in one node by itself. In short, the use of set-oriented bisecting assessment criterion, which does not consider the integrity of each cluster and similarity of clusters within a same subset to determine the split, is a fundamental shortcoming.

To address this fundamental shortcoming, we propose to use a criterion which must preserve each cluster holistically while building a dendrogram. We show that this can be achieved by treating each cluster as a distribution, and using a distributional kernel to perform the bisecting and maintain the integrity of each cluster.

It has been shown [SGSS07] that the feature map of a distributional kernel represents a distribution well. By treating each cluster as a distribution, the use of a distributional kernel to perform bisecting is the key to producing a dendrogram with the three desired properties—avoiding the shortcoming of current methods.

4 Preliminary: Distributional Kernel

Distributional Kernel \mathcal{K} of Kernel Mean Embedding (KME) [SGSS07] is derived using a symmetric and positive definite point kernel κ with feature map ϕ . It represents a distribution \mathcal{P} as a point in Reproducing Kernel Hilbert Space (RKHS) with its feature map $\Phi(\mathcal{P}) = \int_{\mathcal{X}} \kappa(x, \cdot) d\mathcal{P}$, where \mathcal{X} is the support of \mathcal{P} .

Given two datasets X and Y , sampled from distributions \mathcal{P}_X and \mathcal{P}_Y , respectively, the similarity between \mathcal{P}_X and \mathcal{P}_Y can be estimated via KME as $\mathcal{K}(\mathcal{P}_X, \mathcal{P}_Y) = \frac{1}{|X||Y|} \sum_{x \in X, y \in Y} \kappa(x, y) = \langle \Phi(X), \Phi(Y) \rangle$, where the kernel mean map $\Phi(\mathcal{P}_X) = \frac{1}{|X|} \sum_{x \in X} \phi(x)$.

5 Set-Oriented and Distribution-Oriented Approaches to Bisecting in DHC

The two approaches to bisecting to produce a dendrogram T in DHC are defined as follows:

Definition 5.1. Set-oriented approach to bisecting: Given a dataset, each bisecting at an internal node of T splits the set of data points at this node into two subsets based on a bisecting assessment criterion which guides the split by assessing the quality of the split as the dissimilarity between the two subsets (e.g., SpecWRSC) or the cohesiveness of each subset (e.g., Bisect-Kmeans) after each split.

Definition 5.2. Distribution-oriented approach to bisecting: Given a dataset, identify a set C of k core clusters in the first step, and construct a dendrogram T with k leaf nodes from C in the second step. Each bisecting at an internal node of T splits the set of core clusters at this node into two subsets based on a distributional kernel which ensures that similar core clusters are grouped into the same subset.

Although the distribution-oriented approach requires an additional step before constructing a dendrogram, the bisecting in the second step is simpler because it is conducted on a set of k core clusters rather than a set of n data points, where k is a small constant and is independent of dataset size n .

Definition 5.3. A core cluster consists of core points in a cluster which defines the shape, size, and density of the cluster. Non-core or noise points can be eliminated without affecting the cluster being recognized as the same cluster.

Given Definitions 5.2 & 5.3, we show later that the set of core clusters can be identified relatively easily using a small subset of the given dataset. As a result, it provides the first means to a linear-time algorithm.

It is interesting to note that the distributional kernel in the distribution-oriented approach is not a bisecting assessment criterion through which the splitting tries to optimize. The use of distributional kernel and a heuristic and greedy way to assign core clusters during the split provide the second means to a linear-time algorithm.

6 Hierarchical Clustering based on Distributional Kernel

Algorithm 1 H-KC

Hierarchical Clustering based on distributional kernel \mathcal{K}

Input: D - dataset, s - data subset size, k - target number of leaf nodes in the dendrogram, θ - hyperparameters of clustering algorithm \mathcal{A}

Output: Dendrogram T

```

1: Apply  $\mathcal{A}(D_s, k, \theta)$  on subset  $D_s \subset D$ ,  $|D_s| = s$ , to obtain core clusters  $C = \{G_1, G_2, \dots, G_k\}$ .
2: Initialize a binary tree  $T$  with root node as  $C$ .
3: Initialize the set of leaf nodes  $\mathbb{C} = \{C\}$ .
4: while  $|\mathbb{C}| < k$  do
5:   for every leaf node  $\hat{C}$  in  $\mathbb{C}$  do
6:     if the number of core clusters in  $\hat{C}$  is more than 1 then
7:       Split  $\hat{C}$  into subclusters  $C_1$  and  $C_2$ :
        $C_j = \{G \in \hat{C} \mid \arg \max_{i \in [1,2]} \mathcal{K}(\mathcal{P}_G, \mathcal{P}_{\hat{G}_i}) = j\}$ ,
        $\forall_{j \in [1,2]}$ , where  $\hat{G}_1$  and  $\hat{G}_2$  are the two largest core clusters in  $\hat{C}$ .
8:       Update  $\mathbb{C}$  by replacing  $\hat{C}$  with  $C_1$  and  $C_2$  in  $\mathbb{C}$ :  $\mathbb{C} = \mathbb{C} \cup C_1 \cup C_2 \setminus \hat{C}$ .
9:       Expand  $T$ : adding two child nodes  $C_1, C_2$  to  $\hat{C}$ .
10:      end if
11:    end for
12:  end while
13:   $G'_j = \{x \in D \mid \arg \max_{i \in [1,k]} \mathcal{K}(\delta(x), \mathcal{P}_{G_i}) = j\}, \forall_{j \in [1,k]}$ 
14:   $\Delta = \lfloor |D| * 0.01 \rfloor$ ,  $A_j = G_j, \forall_{j \in [1,k]}$ 
15:  for  $t = 1 : 100$  AND  $\sum_j |\{x \mid x \in G'_j, x \notin A_j\}| \geq \Delta$  do
16:     $A_j = G'_j, \forall_{j \in [1,k]}$ 
17:     $G'_j = \{x \in D \mid \arg \max_{i \in [1,k]} \mathcal{K}(\delta(x), \mathcal{P}_{A_i}) = j\}, \forall_{j \in [1,k]}$ 
18:  end for ▷ Refine point assignment
19:  for each core cluster  $G_j$  in each node of  $T$ ,  $G_j \leftarrow G'_j$ .
▷ This step ensures that  $T$  has all the points in  $D$ , not just the core clusters obtained from  $D_s$  in line 1.
20: Return  $T$ .

```

The proposed Hierarchical Clustering based on distributional kernel \mathcal{K} (H-KC) produces a dendrogram T to achieve the objective of maximizing the total similarity of all clusters (TSC):

$$TSC(T) = \sum_{C \in L_T} \sum_{x \in C} \mathcal{K}(\delta(x), \mathcal{P}_C), \quad (1)$$

where L_T represents the set of k leaf nodes of T , and δ denotes a Dirac measure converting a point into a distribution.

The key steps in Algorithm 1 are summarized as follows:

* **Create a set C of k core clusters from D_s** (line 1)

Each element in D_s is sampled from D . An existing clustering algorithm \mathcal{A} can be used here, provided it can find clusters of arbitrary shapes, varied sizes and densities. We show that either psKC [TWZ23] or DBSCAN [EKS⁹⁶] which employs an appropriate kernel can accomplish this task satisfactorily in Appendix D.1.

* **Build a dendrogram T from C** (lines 4-12).

Build a dendrogram from the set of core clusters via bisecting until there are k leaf nodes. Each bisecting selects the largest two core clusters¹ and assigns each other core cluster to one of them based on distributional kernel \mathcal{K} . Note that this process work in a greedy way (unlike existing objective-based DHC methods which exactly optimize a bisecting assessment criterion to build a dendrogram).

* **Assign all points in D to core clusters** (line 13).

Assign each unassigned point in D to the most similar core cluster G_j to get G'_j .

* **Refine point assignment** (lines 14-18).

Refine the assignment of points to improve the total similarity of all clusters (TSC), defined in Equation 1.

* **Finalize nodes in T** (line 19).

Replace core clusters G_j in each node of T with G'_j to ensure that T has all the points in D .

Note that the objectives achieved before and after the refine point assignment step (lines 14-18) have small or no difference. In other words, the refinement often provides tweaks at the edges of clusters in order to find any minor improvement of the objective obtained before.

H- \mathcal{KC} produces dendrogram T with the above-mentioned three desired properties:

1. Once the k core clusters G_i have been identified in line 1 (by algorithm \mathcal{A} which discovers clusters of arbitrary shapes, varied densities and sizes), they remain the same until they are in the k leaf nodes of T (line 12). Every core cluster is not split in any internal node of the dendrogram. So T has the first and third desired properties.
2. Similar clusters are grouped into the same subset, when split at each internal node of T based on their similarity as measured by the distributional kernel (line 7 in Algorithm 1). Therefore, T has the second desired property.

6.1 Dendrogram Created by H- \mathcal{KC} through Local TSC Objective Has a Global Guarantee

Note that the TSC objective considers leaf nodes only in T , and we will refer it as local objective function.

We show that the dendrogram created by H- \mathcal{KC} through the local objective TSC has a global guarantee, i.e., the dendrogram produced by H- \mathcal{KC} has a certain level of quality.

To eliminate the effect of the size of the dataset D , we modify the original local objective TSC into

$$\max_{T \in \mathcal{T}_k} TSC_l(T),$$

where $TSC_l(T) = \frac{1}{|D|} \sum_{C \in L_T} \sum_{x \in C} \mathcal{K}(\delta(x), \mathcal{P}_C)$ is the local objective function for dendrogram T ; L_T is the set of leaf nodes of T ; and \mathcal{T}_k is the set of dendrograms with k leaf nodes, i.e., $|L_T| = k$.

¹Using the two largest core clusters as the basis for each split is an intuitive heuristic which assumes that large clusters are more representative than small clusters.

Although we only refine the local objective TSC_l in H- $\mathcal{K}C$, the dendrogram T created by H- $\mathcal{K}C$ from a given dataset D has a lower bound of the following global objective function TSC_g^p for \mathbb{T}_p , i.e., the set of sub-dendograms having at least p up to k leaf nodes of T :

$$TSC_g^p(T) = \frac{1}{|\mathbb{T}_p|} \sum_{T' \in \mathbb{T}_p} TSC_l(T').$$

When using distributional kernel \mathcal{K} in H- $\mathcal{K}C$ to produce a fixed T of k leaf nodes, and let T^q be a sub-dendrogram of T with $q \leq k$ leaf nodes, $TSC_l(T^q)$ is a monotonically non-increasing function wrt q , as shown in Lemma 6.1.

Lemma 6.1. *For a sub-dendrogram T^q , when contracting any of its two leaf nodes into one to create a new sub-dendrogram T^{q-1} , it holds that*

$$TSC_l(T^{q-1}) \geq TSC_l(T^q) - \alpha,$$

under the assumption that the Euclidean distance between \mathcal{K} 's feature maps of the data distributions in two leaf nodes is less than α , where $\alpha \ll 1$ is a real constant.

Proof. For an internal node of T^q , denote the number of points in its left (right) leaf node as $n_1 = |D_1|$ ($n_2 = |D_2|$), then a contraction of the two leaf nodes into one parent node will decrease $TSC_l(T^q)$ by

$$\begin{aligned} A = & \frac{1}{|D|} \left[\sum_{x \in D_1} \mathcal{K}(\delta(x), P_1) + \sum_{x \in D_2} \mathcal{K}(\delta(x), P_2) \right. \\ & \left. - \sum_{x \in D_1} \mathcal{K}(\delta(x), P') - \sum_{x \in D_2} \mathcal{K}(\delta(x), P') \right], \end{aligned}$$

where P_1 (P_2) is the left (right) leaf node's data distribution having data subset D_1 (D_2). P' is the combination of P_1 and P_2 , having data subset $D_1 \cup D_2$. And $\Phi(P') = \frac{n_1\Phi(P_1) + n_2\Phi(P_2)}{n_1 + n_2}$. Then

$$\begin{aligned} |A| = & \left| \frac{1}{|D|} \left[\frac{n_2}{n_1 + n_2} \sum_{x \in D_1} \langle \Phi(\delta(x)), \Phi(P_1) - \Phi(P_2) \rangle \right. \right. \\ & \left. \left. + \frac{n_1}{n_1 + n_2} \sum_{x \in D_2} \langle \Phi(\delta(x)), \Phi(P_2) - \Phi(P_1) \rangle \right] \right| \\ \leq & \frac{n_2|D_1| + n_1|D_2|}{(n_1 + n_2)|D|} \|\Phi(P_1) - \Phi(P_2)\| \\ \leq & \alpha. \end{aligned}$$

The second line holds because of Cauchy-Schwarz inequality and the norm of \mathcal{K} 's feature map is less than 1. The last line holds based on the assumption stated in the Lemma. Finally, we have $TSC_l(T^{q-1}) \geq TSC_l(T^q) - \alpha$. \square

With Lemma 6.1, we can get the following theorem.

Theorem 6.2. *Under the same assumption in Lemma 6.1, it holds for a dendrogram T with k leaf nodes created by H- $\mathcal{K}C$ that:*

$$\max_{T' \in \mathcal{T}_k} TSC_l(T') - (k-p)\alpha \leq TSC_g^p(T).$$

Proof. A dendrogram with k leaf nodes can contract $k-q$ times to form a sub-dendrogram T^q with q leaf nodes. According to Lemma 6.1, each contraction operation induces a decrease from $\max_{T' \in \mathcal{T}_k} TSC_l(T')$ at most α . Then we have $\max_{T' \in \mathcal{T}_k} TSC_l(T') - (k-q)\alpha \leq TSC_l(T^q)$ for a sub-dendrogram T^q with q leaf nodes of T . By averaging over q (from p to k), we have the stated result in Theorem 6.2. \square

Compared with SpecWRSC (Bisect-Kmeans), which proves that its dendrogram approximates the optimal Dasgupta cost function (Revenue Objective), the dendrogram produced by H- $\mathcal{K}C$ provides a lower bound of TSC_g^p .

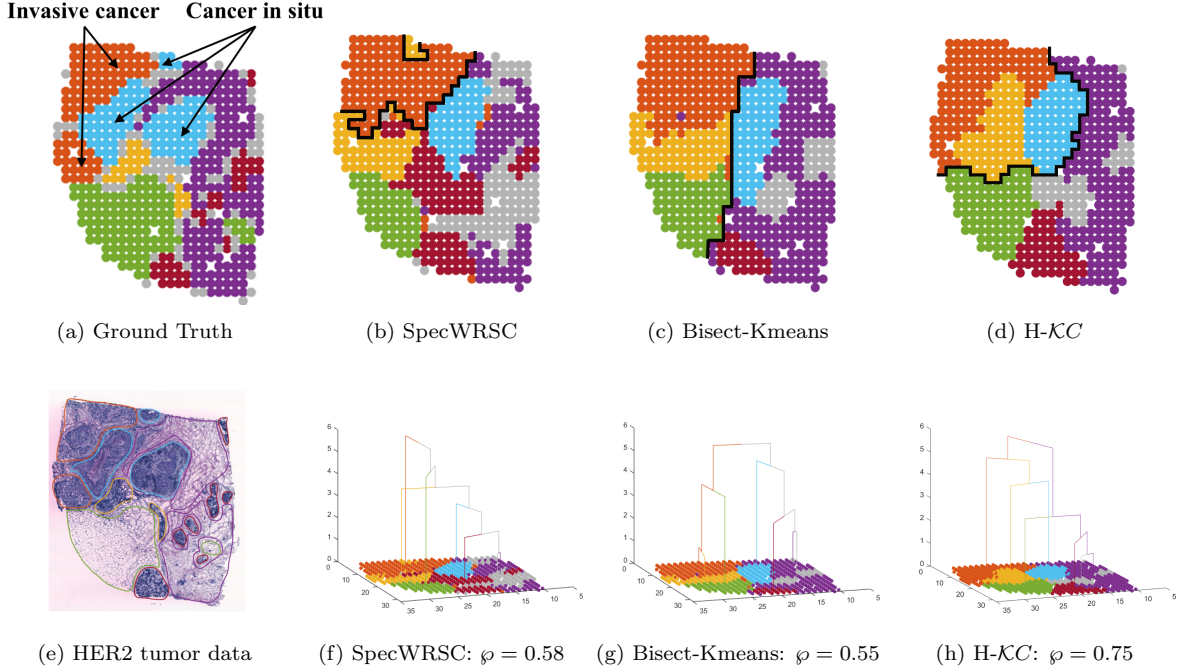


Figure 2: HER2 tumor dataset [ALS⁺20] with ground-truth labels (a) and manual annotation plot of the tissue sample (e). Dendrograms of SpecWRSC (f), Bisect-Kmeans (g) and H-KC (h), and their flat clustering results shown in the leaf nodes are given in (b), (c) and (d), respectively. The solid black line indicates the result of the first split in (b)-(d). The Dendrogram Purity (φ) is calculated in terms of the ‘Invasive cancer’ and ‘Cancer in situ’ regions. The flat clustering result of SpaGCN [HLC⁺21], a recent end-to-end deep learning flat clustering method which produces a comparable flat clustering of Bisect-Kmeans (c), is provided in Appendix D.4.

6.2 H-KC could employ AHC

Proposition 6.3. *With the same set C of core clusters, AHC creates a dendrogram T' similar to T created by H-KC at line 12, if it merges two nodes $X = \{C_{i_1}, \dots, C_{i_m}\}$ and $Y = \{C_{j_1}, \dots, C_{j_n}\}$ with the maximum $f(X, Y) := \max_{C_i \in X, C_j \in Y} \mathcal{K}(C_i, C_j)$.*

Note that f is a single-linkage function that uses \mathcal{K} . Although H-KC does not minimize f in each split, it has an upper bound of f for each split. Therefore, it yields a dendrogram similar to that produced by AHC using the same f , where the arguments in f are clusters/distributions and their similarity is measured by a distributional kernel. The proof is provided in Appendix B.

Proposition 6.3 is consistent with the fact [LLL23, GCB24] that AHC and DHC create the same dendrogram if they use the same single-linkage function to assess the goodness of a merge and a split, respectively. In other words, lines 4-12 in H-KC could use AHC because f is a single-linkage function in terms of distributional kernel; but Bisect-Kmeans and SpecWRSC cannot employ AHC because their objective functions are equivalent to the weighted average linkage function.

The stated procedure (lines 4-12) in Algorithm 1 is preferred over the use of AHC because the former is more efficient to build a dendrogram, i.e., for each split using $f(X, Y)$, where $|X| = |Y| = m$, the time complexity is $O(m)$ for H-KC; but it is $O(m^2)$ for merge using f in AHC.

7 Empirical Evaluation

We evaluate the effectiveness of H-KC in two biological datasets derived from Spatial Transcriptomics [Mar21], which is chosen to be the method of the year in 2021 by Nature Methods. We select these datasets because DHC can potentially provide a deeper insight into the structure of the tissue samples. The first one is the over-expression of HER2 (human epidermal growth factor receptor 2) on tumor cells which identifies two major subtypes of breast cancer. It includes 10053 genes and 607 cells collected through spatial transcriptomics. The second one is the Slide-seq V2 dataset on mouse hippocampus

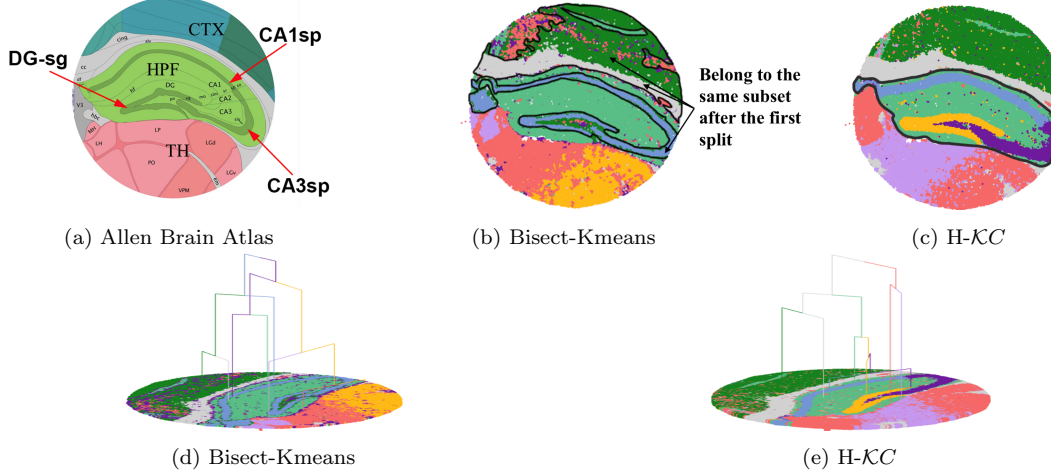


Figure 3: The Slide-seq V2 dataset on mouse hippocampus [SMK⁺21]. Allen Brain Atlas (a) shows the three primary regional divisions: CTX, HPF and TH. The coronal mouse olfactory bulb from the Allen Brain Atlas in the central area is labelled as CA1sp and CA3sp. Dendrograms of Bisect-Kmeans (d) and H- KC (e), and their flat clustering results shown in the leaf nodes are given in (b) and (c), respectively. The solid black line indicates the result of the first split in (b) and the third split in (c).

which contains 53208 cells, each having 23264 genes. Note that Slide-seq V2 does not have ground-truth² label. Each dataset is preprocessed, which integrates the spatial location information of individual cells in a sample tissue and the gene expression information of each cell, into vector representation (HER2 has 120 attributes and 607 points; and Slide-seq V2 has 80 attributes and 51367 points). The details are given in Appendix C.1.

As stated in the Related Work section, since there are no existing metrics to evaluate the quality of a dendrogram’s structure, we use visualization to compare the structures of dendrograms generated by various DHC algorithms.

For the HER2 tumor dataset, the two cancer regions are the center of attention, i.e., ‘Invasive cancer’ and ‘Cancer in situ’, shown in Figure 2a. The observations from the dendrograms produced by Bisect-Kmeans, SpecWRSC and H- KC , shown in Figure 2, are given as follows:

- SpecWRSC produces a highly unbalanced dendrogram which divides a cluster from the rest of the clusters at each internal node. Part of the ‘Cancer in situ’ is mixed with the ‘Invasive cancer’.
- Although both Bisect-Kmeans and H- KC produce rather balanced dendrograms, H- KC has grouped the two cancer regions into the same subset, and the non-cancer regions (regular tissue) into another in the first split; but Bisect-Kmeans divides the two cancer regions into two separate subsets, mixing the cancer and non-cancer regions. In addition, Bisect-Kmeans incorrectly combines ‘Cancer in situ’ with ‘Invasive cancer’, treating them as a single cluster, as SpecWRSC has done. Only H- KC largely correctly identified ‘Invasive cancer’ (into one cluster) and ‘Cancer in situ’ (into two regions). That is the reason why H- KC has significantly higher Dendrogram Purity (ϕ) than SpecWRSC and Bisect-Kmeans.

For Slide-seq V2, the center of attention is the three regions marked as CA1sp, CA3sp and DG-sg in Figure 3a:

- Bisect-Kmeans produces a dendrogram with poor structure: its first split incorrectly groups CA1sp, DG-sg, CA3sp, and CTX into the same subset, as shown in (b). Note that this subset consists of fragment regions separated by regions belonging to another subset. Further, Bisect-Kmeans groups CA1sp, DG-sg and CA3sp at the center of attention into one single cluster in a leaf node.

²This dataset has no ground truth. The Allen Brain Atlas (Figure 3a), which provides the regional divisions, is employed to understand the original tissue structure.

- H- \mathcal{KC} produces a dendrogram that is consistent with the Allen Brain Atlas. The first split separates TH (the bottom region) from CTX & HPF (as a subset). The third split separates HPF from CTX. And the subsequent splits successfully CA1sp, CA3sp ad DG-sg as three different clusters.
- SpecWRSC produces out-of-memory error on this large dataset; thus it has no result in Figure 3.

In summary, both existing objective-based DHC, i.e., SpecWRSC and Bisect-Kmeans, do not produce dendrograms which have the three above-mentioned desired properties. Only H- \mathcal{KC} is capable of generating a dendrogram with a structure that is consistent with the biological regions and accurately detects clusters in the center of attention.

7.1 Comparison with More Baselines

In addition to SpecWRSC and Bisect-Kmeans, we include comparison with more baselines (DHC methods DIANA [KR90], HDP [ZTJA22] and AHC method SCC [MDG⁺21]) on additional 13 datasets. The results in terms of dendrogram purity are shown in Table 3 of Appendix D.6. Here we summarize

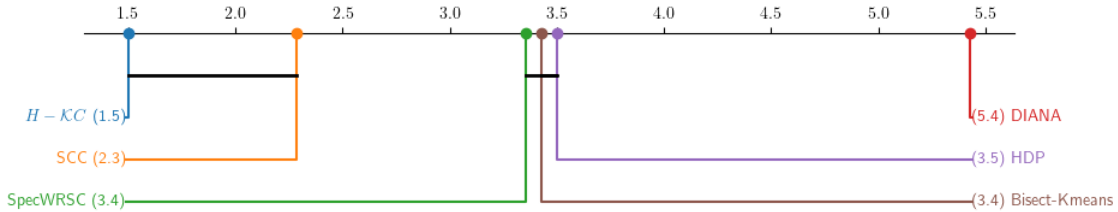


Figure 4: Critical difference diagram.

the results in Appendix D.6 with the corresponding Critical Difference (CD) diagram of the post-hoc Nemenyi test in Figure 4. H- \mathcal{KC} has the highest average ranking and there is no critical difference between H- \mathcal{KC} and SCC. This is consistent with our analysis in Proposition 6.3.

8 Discussion

The time complexity of H- \mathcal{KC} is $\mathcal{O}(kn + s^2)$, where n is the given dataset size, s is the data subset size used to produce the dendrogram (at line 12 in Algorithm 1), and k is the number of leaf nodes. Both Bisect-Kmeans and H- \mathcal{KC} have linear time complexity. The time complexity of SpecWRSC is at least quadratic. The detailed analysis and the scaleup test are given in Appendix D.3.

For the choice of distributional kernel in H- \mathcal{KC} , we use the recently introduced Isolation Distributional Kernel (IDK) [TXWZ20] which can deal with clusters of varied densities better than Gaussian Distributional Kernel (GDK). Our ablation study comparing IDK and GDK in H- \mathcal{KC} is consistent with the previous findings. We have used psKC as \mathcal{A} in line 1 of H- \mathcal{KC} to produce the results in the last section. The examination of different existing algorithms as \mathcal{A} , three ablation studies and a hyperparameter sensitivity analysis of H- \mathcal{KC} are provided in Appendix D.

9 Concluding Remarks

Our discovery of the new approach to objective-based DHC has a much wider implication. Exact optimization on the set-oriented bisecting assessment criterion has been the tool of choice in order to produce an optimized dendrogram. Yet, we show that a greedy algorithm H- \mathcal{KC} exists to lower bound an explicit objective, producing a dendrogram with the three desired properties that existing optimization-based methods could not produce, and H- \mathcal{KC} runs in linear time.

This is possible mainly because of a paradigm shift—the problem is defined in terms of distributions rather than the traditional set-oriented approach. Two key differences are: (I) Bisecting at each internal node of a dendrogram can be better achieved via a distributional kernel, without a typical set-oriented bisecting assessment criterion. The exact optimization of a set-based cost function has no payoff mainly because it does not ensure that similar clusters are grouped in the same subset in each split. (II)

The first step in the distribution-oriented approach in deriving a set of core clusters is crucial in (a) discovering clusters of varying shapes, sizes and densities, and (b) enabling a dendrogram with the three desired properties to be constructed in a new way as stated in (1). We show that this step can be accomplished efficiently from a small subset of a given dataset.

A Background

A.1 Isolation Distributional Kernel

We first describe Isolation Kernel [TZZ18]. Let $D \subset \mathbb{R}^d$ be a dataset sampled from an unknown distribution P_D ; and $\mathbb{H}_\psi(D)$ denote the set of all partitionings H that are admissible from $\mathcal{D} \subset D$, which is a random subset of ψ points. Each partition $\theta[\mathbf{z}] \in H$ isolates a point $\mathbf{z} \in \mathcal{D}$ from the rest of the points in \mathcal{D} . Let $\mathbb{1}(\cdot)$ be an indicator function.

For any two points $x, y \in \mathbb{R}^d$, Isolation Kernel of x and y is defined to be the expectation taken over the probability distribution on all partitionings $H \in \mathbb{H}_\psi(D)$ that both x and y fall into the same isolating partition $\theta[\mathbf{z}] \in H$, where $\mathbf{z} \in \mathcal{D} \subset D$, $\psi = |\mathcal{D}|$:

$$\begin{aligned}\kappa_I(x, y \mid D) &= \mathbb{E}_{\mathbb{H}_\psi(D)}[\mathbb{1}(x, y \in \theta[\mathbf{z}] \mid \theta[\mathbf{z}] \in H)] \\ &= \mathbb{E}_{\mathcal{D} \subset D}[\mathbb{1}(x, y \in \theta[\mathbf{z}] \mid \mathbf{z} \in \mathcal{D})]\end{aligned}$$

In practice, Isolation Kernel κ_I is constructed using a finite number of partitionings $H_i, i = 1, \dots, t$, where each H_i is created using randomly subsampled $\mathcal{D}_i \subset D$; and θ is a shorthand for $\theta[\mathbf{z}]$:

$$\begin{aligned}\kappa_I(x, y \mid D) &= \frac{1}{t} \sum_{i=1}^t \mathbb{1}(x, y \in \theta \mid \theta \in H_i) \\ &= \frac{1}{t} \sum_{i=1}^t \sum_{\theta \in H_i} \mathbb{1}(x \in \theta) \mathbb{1}(y \in \theta)\end{aligned}$$

Let Isolation Kernel be implemented using isolating hyperspheres [TXWZ20] for each partitioning from a sample \mathcal{D} of ψ points. The radius of each hypersphere centered at \mathbf{z} is the distance between \mathbf{z} and its nearest neighbor in $\mathcal{D} \setminus \{\mathbf{z}\}$. Given a partitioning H_i , let feature $\phi_i(x)$ be a ψ -dimensional binary column vector representing all hyperspheres $\theta_j \in H_i, j = 1, \dots, \psi$; where x falls into one of the ψ hyperspheres or none. The j -component of the vector due to H_i is: $\phi_{ij}(x) = \mathbb{1}(x \in \theta_j \mid \theta_j \in H_i)$. Given t partitionings, $\phi(x)$ is the concatenation of $\phi_1(x), \dots, \phi_t(x)$. After that, $\phi(x)$ is divided by \sqrt{t} for normalization such that $\|\phi(x)\| = 1$.

Isolation Distributional Kernel [TXWZ20] is developed from Isolation Kernel κ_I . Since κ_I has finite dimensional feature map ϕ . The feature map of IDK Φ is simply calculated as $\Phi(\mathcal{P}_D) = \frac{1}{|\mathcal{D}|} \sum_{x \in D} \phi(x)$. Since $\|\phi(x)\| = 1$, it holds that $\|\Phi(\mathcal{P}_D)\| \leq 1$.

A.2 Point-Set Kernel Clustering

Point-Set kernel clustering [TWZ23] employs the point-set kernel (distribution kernel where one distribution is a single point) K to characterize clusters. It identifies all members of each cluster by first locating the seed of the dataset. Then, it expands its members in the cluster's local neighborhood which grows at a set rate (ϱ) incrementally; and it stops growing when all unassigned points have similarity w.r.t. the cluster falling below a threshold (τ). The process repeats for the next cluster using the remaining points in the given dataset D , yet to be assigned to any clusters found so far, until D is empty or no point can be found which has similarity more than τ . All remaining points after the clustering process are noise as they are less than the set threshold for each of the clusters discovered. The psKC procedure is shown in Algorithm 2, where K is point-set kernel.

In Algorithm 2, the number of clusters are not automatically determined. In order to fit our setting which takes the number of clusters k as input and incorporate the adaption from point-set kernel to distributional kernel, we introduce distributional kernel based psKC (\mathcal{K} -psKC) in Algorithm 3, where \mathcal{K} represents distributional kernel. We apply Algorithm 3 on a subset of the entire dataset to obtain k core clusters in the first line of H- \mathcal{K} C. The noise set N is not part of the core clusters.

A.3 Dendrogram Purity

Given a dendrogram T produced by a hierarchical clustering algorithm from a dataset $D = \{\mathbf{x}_1, \dots, \mathbf{x}_n\}$. Let $\mathsf{P} = \{(\mathbf{x}, \mathbf{x}') \mid \mathbf{x} \neq \mathbf{x}' \in D, \ell(\mathbf{x}) = \ell(\mathbf{x}')\}$ be the set of pairs of different points that have the same

Algorithm 2 point-set Kernel Clustering (psKC)

Input: D : dataset, τ : similarity threshold, ϱ : growth rate

Output: $G^j, j = 1, \dots, k$: k clusters, N : noise set

```

1:  $k = 0$ 
2: while  $|D| > 1$  do
3:    $x_p = \arg \max_{x \in D} K(x, D)$  ▷ Seed
4:    $x_q = \arg \max_{x \in D \setminus \{x_p\}} K(x, \{x_p\})$ 
5:    $\gamma = (1 - \varrho) \times K(x_q, \{x_p\})$ 
6:   if  $\gamma \leq \tau$  then
7:     Terminate while-do loop
8:   end if
9:    $k++$ 
10:   $G_0^k = \{x_p, x_q\}$  ▷ Initial cluster  $k$ 
11:  for  $(i = 1; \gamma > \tau; i++)$  do
12:     $G_i^k = \{x \in D \mid K(x, G_{i-1}^k) > \gamma\}$ 
13:     $\gamma = (1 - \varrho)\gamma$ 
14:  end for
15:   $G^k = G_{i-1}^k$  ▷ Cluster  $k$  grown
16:   $D = D \setminus G^k$ 
17: end while
18:  $N = D$ 
19: Return  $G^j, j = 1, \dots, k; N$ 

```

ground-truth cluster label, where $\ell(\mathbf{x})$ denotes the ground-truth cluster label of \mathbf{x} ; and $L_i, i = 1, \dots, \mathbf{k}$ be the ground-truth labels of \mathbf{k} clusters. Formally, the *Dendrogram Purity* of T is defined as [KMKM17]

$$\text{Purity}(T) = \frac{1}{|\mathbf{P}|} \sum_{i=1}^{\mathbf{k}} \sum_{(\mathbf{x}, \mathbf{x}') \in \mathbf{P}, \ell(\mathbf{x})=L_i} \mathfrak{f}(\mathfrak{g}(\mathfrak{h}(\mathbf{x}, \mathbf{x}')), L_i),$$

where $\mathfrak{h}(\mathbf{x}, \mathbf{x}')$ is the least common ancestor of \mathbf{x} and \mathbf{x}' in \mathbb{T} , $\mathfrak{g}(\mu) \subset D$ is the set of points in all the descendant leaf nodes of internal node μ in T , and $\mathfrak{f}(S, L_i) = \frac{|\{\mathbf{x} \in S \mid \ell(\mathbf{x})=L_i\}|}{S}$ computes the fraction of S that matches the ground-truth label L_i .

B Proof

Proposition B.1. *With the same leaf nodes of dendrogram T created by H-KC, AHC creates a similar dendrogram T' , if it merges two nodes $X = \{C_{i_1}, \dots, C_{i_m}\}$ and $Y = \{C_{j_1}, \dots, C_{j_n}\}$ with the maximum $f(X, Y) := \max_{C_i \in X, C_j \in Y} \mathcal{K}(C_i, C_j)$.*

Proof. AHC and DHC create the same dendrogram [LLL23, GCB24] if they use the same single-linkage function f to assess the goodness of a merge and a split, respectively. That is, if AHC merges the two most similar nodes at each step according to $f(X, Y)$, which have subsets X and Y , then a DHC algorithm produces the same dendrogram if every bisecting minimizes $f(X, Y)$.

Let $f(X, Y) = \max_{C_i \in X, C_j \in Y} \mathcal{K}(\mathcal{P}_{C_i}, \mathcal{P}_{C_j})$, where \mathcal{K} is a distribution kernel. The following AHC and DHC algorithms produce the same dendrogram:

- * AHC merges two nodes $X = \{C_{i_1}, \dots, C_{i_m}\}$ and $Y = \{C_{j_1}, \dots, C_{j_n}\}$ with the maximum $f(X, Y)$.
- * DHC minimizes $f(X, Y)$ when it splits a node into two child nodes X, Y .

Note that the bisecting criterion of H-KC, i.e., $\{G \in \hat{C} \mid \arg \max_{i \in [1,2]} \mathcal{K}(\mathcal{P}_G, \mathcal{P}_{\hat{G}_i}) = j\}$, does not choose the best split among many possible splits, but it simply divides the set \hat{C} into two subsets based on the two largest core clusters \hat{G}_1, \hat{G}_2 . In other words, the criterion is not an assessment function. Hence, H-KC does not produce the same dendrogram as that produced by AHC or DHC with f .

Algorithm 3 Distributional kernel based psKC (\mathcal{K} – psKC)

Input: D : dataset, k : number of clusters, τ : similarity threshold, ϱ : growth rate

Output: $G^j, j = 1, \dots, k$: k clusters

```

1:  $j = 0$ 
2: while  $|D| > 1$  and  $j < k$  do
3:    $x_p = \arg \max_{x \in D} \mathcal{K}(\delta(x), P_D)$  ▷ Seed
4:    $x_q = \arg \max_{x \in D \setminus \{x_p\}} \mathcal{K}(\delta(x), \delta(x_p))$ 
5:    $\gamma = (1 - \varrho) \times \mathcal{K}(\delta(x_q), \delta(x_p))$ 
6:   if  $\gamma \leq \tau$  then
7:     Terminate while-do loop
8:   end if
9:    $j++$ 
10:   $G_0^j = \{x_p, x_q\}$  ▷ Initial cluster  $k$ 
11:  for  $(i = 1; \gamma > \tau; i++)$  do
12:     $G_i^j = \{x \in D \mid \mathcal{K}(\delta(x), P_{G_{i-1}^j}) > \gamma\}$ 
13:     $\gamma = (1 - \varrho)\gamma$ 
14:  end for
15:   $G^j = G_{i-1}^j$  ▷ Cluster  $j$  grown
16:   $D = D \setminus G^j$ 
17: end while
18: Return  $\{G^1, G^2, \dots, G^k\}$ .

```

Although H- $\mathcal{K}C$ does not minimize f , the bisecting criterion provides an upper-bound for f , i.e., $f(X, Y) \leq \tau$, where τ is the similarity threshold in \mathcal{K} -psKC, i.e. the default choice in the first line of H- $\mathcal{K}C$.

□

C Data and Experiment Settings

C.1 Spatial Transcriptomics data

The HER2 breast tumor dataset was downloaded from github: <https://github.com/almaan/her2st>. The dataset contains eight samples with pathologist-annotated labels, and we used the H1 sample to demonstrate the result.

Mouse hippocampus Slide-seq V2 data were downloaded from the Single Cell Portal SCP815 website: https://singlecell.broadinstitute.org/single_cell/study/SCP815/sensitive-spatial-genome-wide-782.

We used the file “Puck_200115_08” in our study. The dataset contains approximately 23,000 genes and 53,000 spatial locations.

Begin with a spatial transcriptomics dataset, we normalized the raw molecular count matrix using the variance stabilizing transformation method called SCTransform [CS22]. To select spatially variable genes, we apply SPARK [SZZ20] in the HER2 breast tumor dataset and use SPARK-X [ZSZ21] in the mouse hippocampus Slide-seq V2 data, as conducted in previous studies. Then the cell spatial information and the gene expression information are integrated to produce a graph. Then, a graph embedding scheme called the Weisfeiler-Lehman scheme [SSVL+11] converts a graph into a vector representation. The Weisfeiler–Lehman(WL) embedding used here is the same as that proposed by [TGLL+19]. For a graph $G = (V, E)$ with continuous attributes $a(v) \in \mathbb{R}^m$, the WL embedding at iteration $h > 0$ is recursively defined as:

$$a^{h+1}(v) = \frac{1}{2} \left(a^h(v) + \frac{1}{\deg(v)} \sum_{u \in \mathcal{N}(v)} w((v, u)) \cdot a^h(u) \right).$$

When edge weights are not available, $w((u, v))$ is set to 1. Using the recursive procedure described above, a WL-based graph embedding scheme that generates node embeddings from the attributes of

the graphs can be proposed as

$$\Phi(v) = [a^0(v), \dots, a^h(v)]^\top.$$

Then, for a graph $G = (V, E)$, its mean embedding or its feature mean map is given as

$$\hat{\Phi}(G) = \frac{1}{|V|} \sum_{v \in V} \Phi(v) = \frac{1}{|V|} \sum_{v \in V} [a^0(v), \dots, a^h(v)]^\top.$$

C.2 Machine and hyperparameter settings

The experiments are performed on a machine with 2.20GHz CPU and 16GB RAM. The search range of hyperparameter is provided in Table 1.

Table 1: Hyperparameter search range.

| | search range |
|-------------------|---|
| Isolation Kernel | $\psi \in \{4, 6, 8, 16, 24, 32, 48\}, t = 200$ |
| H- \mathcal{KC} | $\tau \in [0.1, 0.5, 1, 5, 10, 50, 100, 500, 1000] \times 10^{-4}$ $\rho = 0.1$ |
| WL | $h = 7$ |
| SpaGCN | $histology \in \{true, false\}$ $init \in \{"louvain", "kmeans"\}$ |

D Additional Experiments

D.1 Ablation studies

For the choice of distributional kernel, we consider recently introduced Isolation Distributional Kernel (IDK) [TXWZ20], which origins from Isolation Kernel [TZ18] and has finite dimensional feature map.

In the first ablation study, we compare IDK with Gaussian Distributional Kernel (GDK) in Figure 5. This one needs to modify the affect lines 1, 7, 13 & 17, where distributional kernel is used. In lines 1, 7, 13 & 17, distribution kernel employs the same hyperparameter. As shown in Figure 5. IDK successfully identifies three Gaussian distributions with varied densities and the clusters, in contrast to GDK which is unable to achieve this. GDK also can not correctly identify the two clusters on the bottom. In addition, after the first split, the leftmost Gaussian cluster is in the same subset with the L-shape cluster, instead of the middle Gaussian cluster.

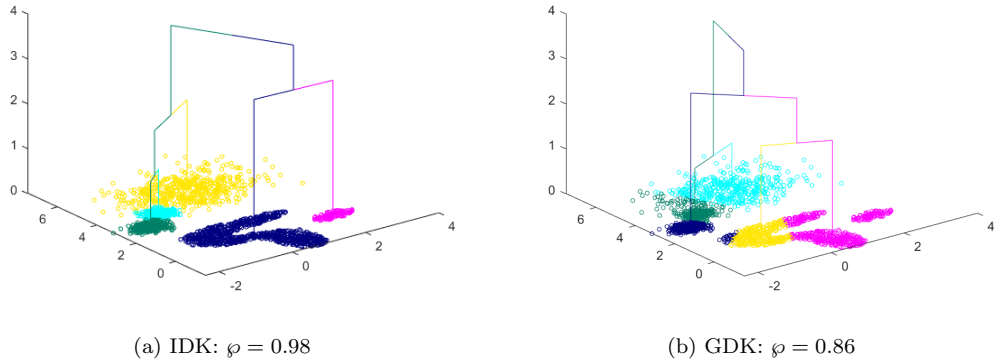


Figure 5: Results of IDK vs GDK in H- \mathcal{KC} on the artificial dataset. ϕ is Dendrogram Purity (DP).

The second ablation study examines the utility of the point-re-assignment (post-processing: line 14-18 in H- \mathcal{KC}). The refinement or post-processing often provides tweaks at the edges of clusters. As

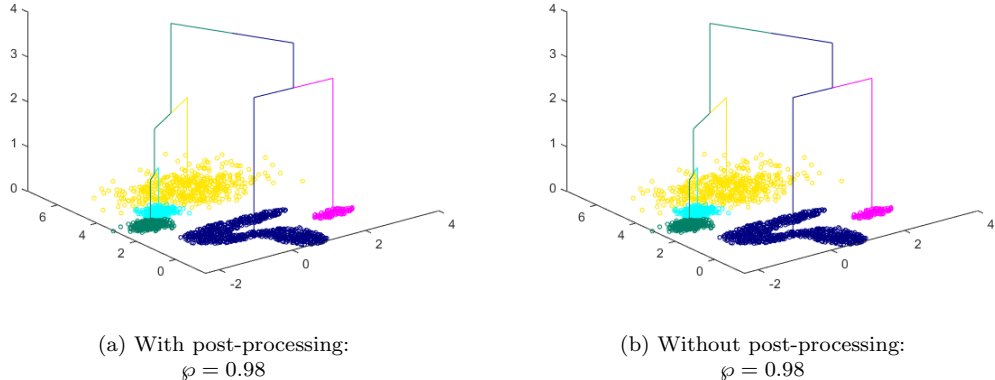


Figure 6: Results of with and without post-processing.

as a consequence, the results with and without post-processing are basically the same on the artificial dataset, as shown in Figure 6.

In the third ablation study, we consider three different clustering choices, \mathcal{K} -psKC, k-means [ASI20] and DBSCAN [EKS⁺96] in line 1 of H- \mathcal{KC} . The results are shown in Figure 7. For k-means and DBSCAN, we also consider their variants that uses Isolation Kernel (IK) [TZZ18] as similarity measure. DBSCAN with IK can successfully identifies the clusters and produce the same dendrogram as that produced by \mathcal{K} -psKC.

In the last ablation study, we consider constructing the dendrogram with AHC. We replace line 4-12 of H- \mathcal{KC} by using $h(X, Y) = \max_{C_i \in X, C_j \in Y} \mathcal{K}(\mathcal{P}_{C_i}, \mathcal{P}_{C_j})$ for the merge of core clusters. The resultant dendrogram is exactly the same as that produced by H- \mathcal{KC} in Figure 5a. This result is consistent with our analysis in Proposition 1.

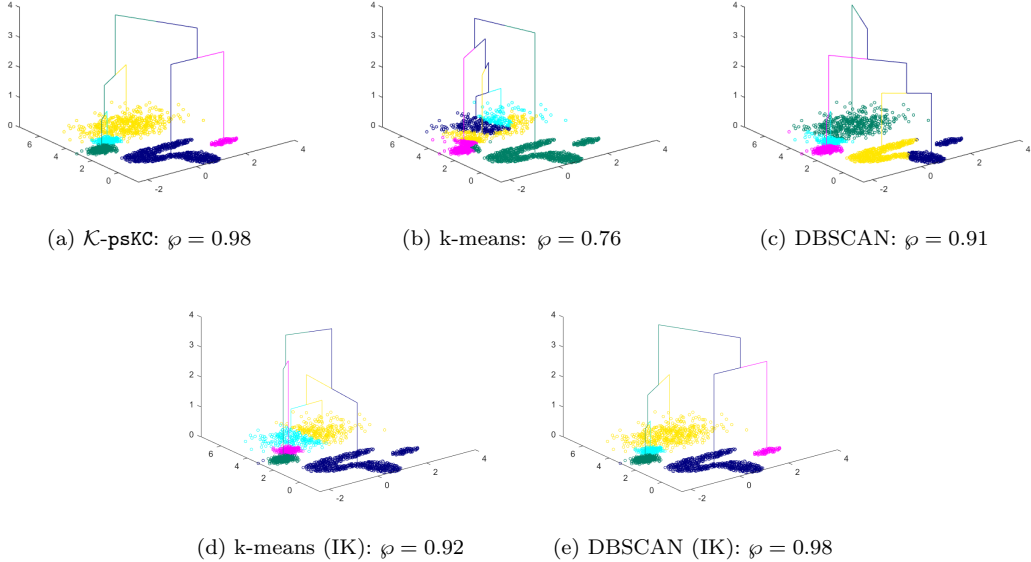


Figure 7: Results of different clustering method in line 1 of H- \mathcal{KC} .

D.2 SpecWRSC using psKC for initial clusters

We present the results of SpecWRSC with psKC (instead of Spectral Clustering) as the initial clusters in Figure 8.

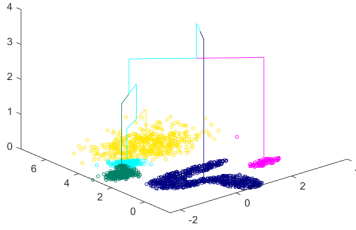


Figure 8: SpecWRSC using psKC for initial clusters: $\varphi = 0.95$

D.3 Scaleup test

The time complexity of H-KC is $\mathcal{O}(kn + s^2)$, where n is the data size, s is the data subset size and k is the number of leaf nodes. Bisect-Kmeans has $\mathcal{O}(knR)$ time complexity, where R is the number of repeated Kmeans. SpecWRSC has time complexity of $G + \mathcal{O}(m \log^c n)$, where G and m are the time to build a graph and the number of edges in the graph, respectively. The time complexity of G varies in the range $[\mathcal{O}(n), \mathcal{O}(n^2)]$, depending on the implementation. c is a constant greater than 1. The scaleup test results, shown in Figure 9, are consistent with their time complexities.

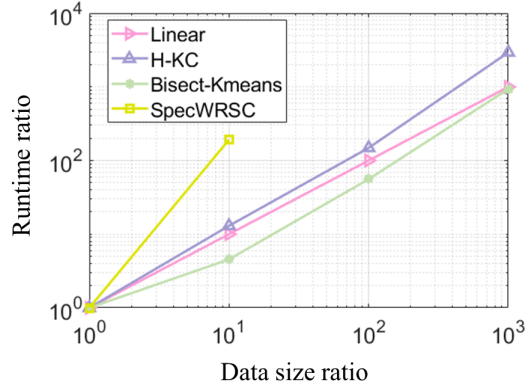


Figure 9: Scaleup test result on the same artificial dataset used in the main paper, where the data set size has 3000 points at data size ratio = 1.

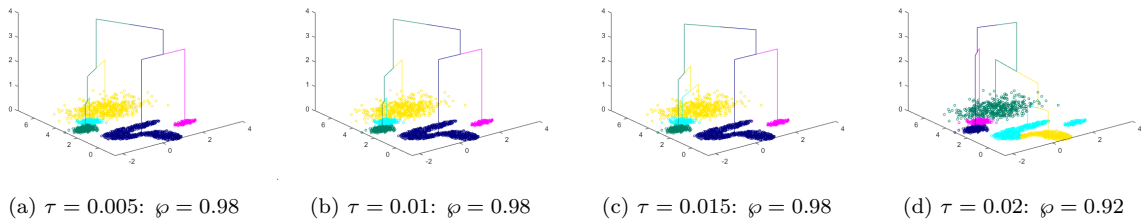
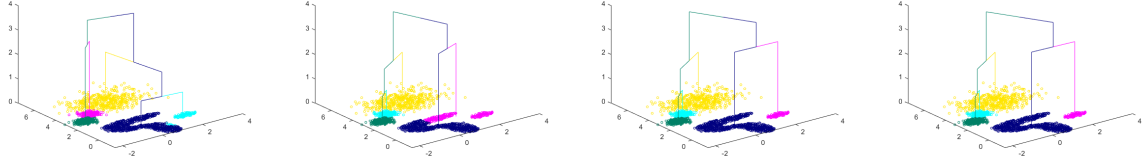


Figure 10: Dendrograms of H-KC on the artificial dataset under different similarity thresholds τ .

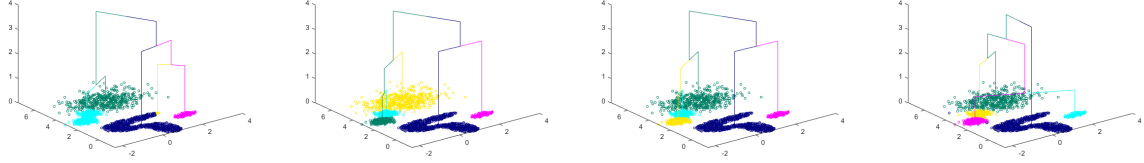
D.4 Flat clustering of SpaGCN on HER2

Here we use SpaGCN [HLC⁺21], an end-to-end deep learning method, to perform flat clustering on the HER2 dataset, and it achieves NMI=0.45 and ARI=0.32. The clustering result is shown in Figure



(a) $s = 1250$: $\varphi = 0.97$ (b) $s = 1500$: $\varphi = 0.95$ (c) $s = 1750$: $\varphi = 0.98$ (d) $s = 2129$: $\varphi = 0.98$

Figure 11: Dendrograms of H- \mathcal{KC} on the artificial dataset under different data subset size s .



(a) $\psi = 40$: $\varphi = 0.85$ (b) $\psi = 60$: $\varphi = 0.98$ (c) $\psi = 80$: $\varphi = 0.98$ (d) $\psi = 100$: $\varphi = 0.97$

Figure 12: Dendrograms of H- \mathcal{KC} on the artificial dataset under different ψ values.

13. The results of Bisect-Kmeans, SpecWRSC and H- \mathcal{KC} are provided in Table 2. Bisect-Kmeans is comparable to SpaGCN. H- \mathcal{KC} outperforms the other methods.

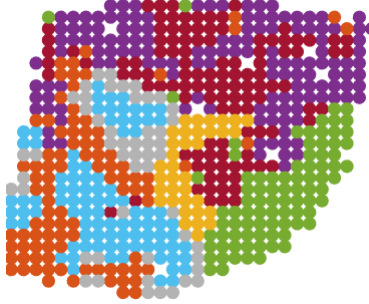


Figure 13: SpaGCN’s clustering result on the HER2 dataset.

Table 2: Normalized Mutual Information (NMI) and Adjusted Rand Index (ARI) of different clustering algorithms. For DHC methods (Bisect-Kmeans, SpecWRSC and H- \mathcal{KC}), we use their leaf nodes as the final clustering result.

| | SpaGCN | Bisect-Kmeans | SpecWRSC | H- \mathcal{KC} |
|-----|--------|---------------|----------|-------------------|
| NMI | 0.45 | 0.46 | 0.41 | 0.48 |
| ARI | 0.32 | 0.39 | 0.26 | 0.43 |

D.5 Sensitivity analysis

Here we perform sensitivity analysis about the hyperparameters of H- \mathcal{KC} and distributional kernel (Isolation Distributional Kernel) on the same artificial dataset. We adjust the hyperparameter within a small range near the optimal value $\tau = 0.01, \psi = 64$.

- For the similarity threshold τ , it’s more sensitive when τ is relatively large. It is robust in a small range around the optimal choice $\tau = 0.1$, as shown in Figure 10.

- For the data subset size s , it is more robust when s is large. When s is small, the consequent core clusters are not representative enough to produce good clustering result, as shown in Figure 11.
- For the hyperparameter ψ in Isolation Distributional Kernel (IDK), ψ is a data-dependent hyperparameter, it is robust in a small range around the optimal choice $\psi = 64$ (from 48 to 80), as shown in Figure 12.

D.6 Comparison with more baselines

In addition to SpecWRSC and Bisect-Kmeans, we include comparison with more baselines (DHC methods DIANA [KR90], HDP [ZTJA22] and AHC method SCC [MDG⁺21]) on additional 13 datasets. We report dendrogram purity in Table 3.

Table 3: Hierarchy clustering results in terms of dendrogram purity. **NC** indicates that the run could not be completed within one day.

| Dataset | DHC | | | | | AHC |
|--------------|------|---------------|-------|----------|-----|------|
| | H-KC | Bisect-Kmeans | DIANA | SpecWRSC | HDP | |
| ALLAML | .73 | .71 | .63 | .72 | .73 | .74 |
| LSVT | .74 | .64 | .59 | .70 | .65 | .66 |
| Wine | .95 | .84 | .42 | .95 | .83 | .95 |
| Seeds | .87 | .84 | .41 | .88 | .82 | .85 |
| Musk | .57 | .54 | .51 | .57 | .54 | .54 |
| WDBC | .90 | .88 | .58 | .88 | .84 | .92 |
| LandCover | .55 | .53 | .22 | .49 | .43 | .60 |
| Banknote | .97 | .63 | .51 | .60 | .98 | .90 |
| Spam | .84 | .68 | .54 | .70 | .57 | .68 |
| ImageNet-10 | .84 | .80 | .10 | .78 | .84 | .86 |
| STL-10 | .63 | .59 | .10 | .50 | .59 | .59 |
| CIFAR-10 | .66 | .64 | .10 | NC | .64 | .63 |
| MNIST | .54 | NC | .69 | NC | NC | .39 |
| Covertype | .49 | .46 | NC | NC | NC | .45 |
| Avg. ranking | 1.50 | 3.43 | 5.43 | 3.36 | 3.5 | 2.29 |

References

[ALS⁺20] Alma Andersson, Ludvig Larsson, Linnea Stenbeck, Fredrik Salmén, Anna Ehinger, Sunny Wu, Ghamdan Al-Eryani, Daniel Roden, Alex Swarbrick, Åke Borg, et al. Spatial deconvolution of her2-positive breast tumors reveals novel intercellular relationships. *bioRxiv*, 2020.

[ASI20] Mohiuddin Ahmed, Raihan Seraj, and Syed Mohammed Shamsul Islam. The k-means algorithm: A comprehensive survey and performance evaluation. *Electronics*, 9(8):1295, 2020.

[Bol98] Daniel Boley. Principal direction divisive partitioning. *Data Mining and Knowledge Discovery*, 1998.

[CAKMT17] Vincent Cohen-Addad, Varun Kanade, and Frederik Mallmann-Trenn. Hierarchical clustering beyond the worst-case. *Advances in Neural Information Processing Systems*, 2017.

[CAKMTM19] Vincent Cohen-Addad, Varun Kanade, Frederik Mallmann-Trenn, and Claire Mathieu. Hierarchical clustering: Objective functions and algorithms. *Journal of the ACM*, 2019.

[CNC18] Vaggos Chatziafratis, Rad Niazadeh, and Moses Charikar. Hierarchical clustering with structural constraints. *International Conference on Machine Learning*, 2018.

[CS22] Saket Choudhary and Rahul Satija. Comparison and evaluation of statistical error models for scRNA-seq. *Genome Biology*, 23(1):27, 2022.

[Das16] Sanjoy Dasgupta. A cost function for similarity-based hierarchical clustering. In *Proceedings of the forty-eighth annual ACM symposium on Theory of Computing*, 2016.

[DBE⁺15] Ibai Diez, Paolo Bonifazi, Iñaki Escudero, Beatriz Mateos, Miguel A Muñoz, Sebastiano Stramaglia, and Jesus M Cortes. A novel brain partition highlights the modular skeleton shared by structure and function. *Scientific Reports*, 2015.

[EKS⁺96] Martin Ester, Hans-Peter Kriegel, Jörg Sander, Xiaowei Xu, et al. A density-based algorithm for discovering clusters in large spatial databases with noise. In *Proceedings of the ACM SIGKDD International Conference on Knowledge Discovery and Data Mining*, volume 96, pages 226–231, 1996.

[FZCW21] Zhiqiang Fu, Yao Zhao, Dongxia Chang, and Yiming Wang. A hierarchical weighted low-rank representation for image clustering and classification. *Pattern Recognition*, 2021.

[GCBB24] Marek Gagolewski, Anna Cena, Maciej Bartoszuk, and Łukasz Brzozowski. Clustering with minimum spanning trees: How good can it be? *Journal of Classification*, pages 1–23, 2024.

[GPvL19] Debarghya Ghoshdastidar, Michaël Perrot, and Ulrike von Luxburg. Foundations of comparison-based hierarchical clustering. *Advances in Neural Information Processing Systems*, 2019.

[HG05] Katherine A Heller and Zoubin Ghahramani. Bayesian hierarchical clustering. *International Conference on Machine Learning*, 2005.

[HLC⁺21] Jian Hu, Xiangjie Li, Kyle Coleman, Amelia Schroeder, Nan Ma, David J Irwin, Edward B Lee, Russell T Shinohara, and Mingyao Li. Spagn: Integrating gene expression, spatial location and histology to identify spatial domains and spatially variable genes by graph convolutional network. *Nature Methods*, 2021.

[Hub73] Lawrence Hubert. Monotone invariant clustering procedures. *Psychometrika*, 1973.

[KMKM17] Ari Kobren, Nicholas Monath, Akshay Krishnamurthy, and Andrew McCallum. A hierarchical algorithm for extreme clustering. In *Proceedings of the 23rd ACM SIGKDD International Conference on Knowledge Discovery & Data Mining*, 2017.

[KR90] L. Kaufman and P.J. Rousseeuw. *Chapter 6. Divisive Analysis (Program DIANA)*. In *Finding Groups in Data: An Introduction to Cluster Analysis*. 1990.

[LBWX19] Chunlin Li, Jingpan Bai, Zhao Wenjun, and Yang Xihao. Community detection using hierarchical clustering based on edge-weighted similarity in cloud environment. *Information Processing & Management*, 2019.

[LLL23] Martine Labb , Mercedes Landete, and Marina Leal. Dendograms, minimum spanning trees and feature selection. *European Journal of Operational Research*, 308(2):555–567, 2023.

[LMS23] Steinar Laenen, Bogdan Adrian Manghiuc, and He Sun. Nearly-optimal hierarchical clustering for well-clustered graphs. *International Conference on Machine Learning*, 2023.

[Mar21] Vivien Marx. Method of the year spatially resolved transcriptomics. *Nature Methods*, 2021.

[MDG⁺21] Nicholas Monath, Kumar Avinava Dubey, Guru Guruganesh, Manzil Zaheer, Amr Ahmed, Andrew McCallum, Gokhan Mergen, Marc Najork, Mert Terzihan, Bryon Tjanaka, Yuan Wang, and Yuchen Wu. Scalable hierarchical agglomerative clustering. In *Proceedings of the 27th ACM SIGKDD Conference on Knowledge Discovery & Data Mining*, KDD '21, page 1245–1255, New York, NY, USA, 2021. Association for Computing Machinery.

[MSWDM64] P Macnaughton-Smith, WT Williams, MB Dale, and LG Mockett. Dissimilarity analysis: a new technique of hierarchical sub-division. *Nature*, 1964.

[NG06] Boaz Nadler and Meirav Galun. Fundamental limitations of spectral clustering. In *Proceedings of the 19th International Conference on Neural Information Processing Systems*, pages 1017–1024, 2006.

[NYA21] Stanislav Naumov, Grigory Yaroslavtsev, and Dmitrii Avdiukhin. Objective-based hierarchical clustering of deep embedding vectors. In *Proceedings of the AAAI Conference on Artificial Intelligence*, 2021.

[PZZ⁺22] Yue Pang, Xiangdong Zhou, Junqi Zhang, Quan Sun, and Jianbin Zheng. Hierarchical electricity time series prediction with cluster analysis and sparse penalty. *Pattern Recognition*, 2022.

[RP17] Aurko Roy and Sebastian Pokutta. Hierarchical clustering via spreading metrics. *Journal of Machine Learning Research*, 2017.

[SGSS07] Alex Smola, Arthur Gretton, Le Song, and Bernhard Schölkopf. A hilbert space embedding for distributions. *International Conference on Algorithmic Learning Theory*, 2007.

[SJ⁺22] Arun Kumar Sangaiah, Amir Javadpour, Forough Ja'fari, Weizhe Zhang, and Shadi Mahmoodi Khaniabadi. Hierarchical clustering based on dendrogram in sustainable transportation systems. *IEEE Transactions on Intelligent Transportation Systems*, 2022.

[SKK00] M. Steinbach, G. Karypis, and V. Kumar. A comparison of document clustering techniques. *KDD Workshop on Text Mining*, 2000.

[SMK⁺21] Robert R Stickels, Evan Murray, Pawan Kumar, Jilong Li, Jamie L Marshall, Daniela J Di Bella, Paola Arlotta, Evan Z Macosko, and Fei Chen. Highly sensitive spatial transcriptomics at near-cellular resolution with slide-seqv2. *Nature Biotechnology*, 2021.

[SSVL⁺11] Nino Shervashidze, Pascal Schweitzer, Erik Jan Van Leeuwen, Kurt Mehlhorn, and Karsten M Borgwardt. Weisfeiler-lehman graph kernels. *Journal of Machine Learning Research*, 12(9), 2011.

[SZZ20] Shiquan Sun, Jiaqiang Zhu, and Xiang Zhou. Statistical analysis of spatial expression patterns for spatially resolved transcriptomic studies. *Nature Methods*, 17(2):193–200, 2020.

[TGLL⁺19] Matteo Togninalli, Elisabetta Ghisu, Felipe Llinares-López, Bastian Rieck, and Karsten Borgwardt. Wasserstein weisfeiler-lehman graph kernels. *Advances in Neural Information Processing Systems*, 32, 2019.

[TLM10] Michele Tumminello, Fabrizio Lillo, and Rosario N. Mantegna. Correlation, hierarchies, and networks in financial markets. *Journal of Economic Behavior & Organization*, 2010.

[TWZ23] Kai Ming Ting, Jonathan R. Wells, and Ye Zhu. Point-set kernel clustering. *IEEE Trans. on Knowl. and Data Eng.*, 35(5):5147–5158, May 2023.

[TXWZ20] Kai Ming Ting, Bi-Cun Xu, Takashi Washio, and Zhi-Hua Zhou. Isolation distributional kernel: A new tool for kernel based anomaly detection. In *Proceedings of the 26th ACM SIGKDD International Conference on Knowledge Discovery & Data Mining*, 2020.

- [TZZ18] Kai Ming Ting, Yue Zhu, and Zhi-Hua Zhou. Isolation kernel and its effect on svm. *Proceedings of the 24th ACM SIGKDD International Conference on Knowledge Discovery & Data Mining*, 2018.
- [VL07] Ulrike Von Luxburg. A tutorial on spectral clustering. *Statistics and Computing*, 2007.
- [WM20] Yuyan Wang and Benjamin Moseley. An objective for hierarchical clustering in euclidean space and its connection to bisecting k-means. In *Proceedings of the AAAI Conference on Artificial Intelligence*, 2020.
- [ZSZ21] Jiaqiang Zhu, Shiquan Sun, and Xiang Zhou. Spark-x: non-parametric modeling enables scalable and robust detection of spatial expression patterns for large spatial transcriptomic studies. *Genome Biology*, 22(1):184, 2021.
- [ZTJA22] Ye Zhu, Kai Ming Ting, Yuan Jin, and Maia Angelova. Hierarchical clustering that takes advantage of both density-peak and density-connectivity. *Information Systems*, 103:101871, 2022.